White Rose seismic with well data constraints: A case history

Ayiaz Kaderali, Husky Energy, St. John's, Canada
Michael Jones, Schlumberger, Calgary, Canada
Jonathan Howlett, WesternGeco, Calgary, Canada

Interpreters are always seeking improvements to seismic data in quality, resolution, and the accuracy with which the data represent the underlying geology. Consistency of the seismic image with known control points, usually wells, is essential. The bridge between the high-resolution, geographically sparse, depth-indexed world of logs and the low-resolution, geographically ubiquitous and time-indexed world of seismic is the vertical seismic profile (VSP) in its various geometries.

At White Rose, field development has been proceeding for several years and a reasonable amount of well control is available, including several VSP data sets. A project was undertaken to reprocess the surface seismic data over the White Rose Field and some adjoining acreage with the objective of honoring the well data and borehole-derived parameters to arrive at a processing flow that would result in the most accurate and interpretable data cube possible.

Some concerns, and the ways in which borehole seismic can be used to ameliorate them, are shown in Table 1. Understanding the details of the velocity field is key for several processes. Borehole seismic provides the necessary data to calibrate the sonic logs, measure Q, and measure interval and effective anisotropy. Even if the velocity field is only known in detail at discrete well locations, it can provide a significant constraint over a much larger area. Examples exist in the literature demonstrating the use of calibrated, detailed velocity models for accurate gain recovery, true amplitude processing, long-offset AVO, and improved imaging.

Background. The offshore White Rose oil field, in the Jeanne d'Arc Basin, is approximately 350 km east of St. John's, Newfoundland and Labrador, Canada. It is about 50 km east of the Hibernia Field and about 50 km northeast of the Terra Nova Field (Figure 1).

The field was discovered in 1984, and consists of both oil and gas pools. The oil pool covers approximately 40 km^2 and contains an estimated 200–250 million barrels of recoverable oil.

The Jeanne d'Arc Basin is an extensional basin formed during the Mesozoic Era, dominated by listric and high-angle normal faults. The tectonic history of the area includes three rifting events with significant thermal subsidence during Late Jurassic-Early Cretaceous times followed by pronounced, strictly thermal subsidence during the Late Cretaceous and Tertiary (Enachescu, 1987).

The White Rose region lies in the easternmost part of the Jeanne d'Arc Basin (Figure 2). Figure 3 is a map of the region;

Table 1. *Problems and their borehole-referenced seismic solutions.*

Problem	Borehole-referenced seismic solution
Multiples	• 1D calibrated anisotropic velocity model • Peg-leg multiple prediction • Water-bottom reflectivity determination • Velocity control
Resolution	• Attenuation compensation Q • Wavelet matching • 1D calibrated anisotropic velocity model
Imaging	• 1D calibrated anisotropic velocity model
AVO consistency	• Offset-dependant gain and spreading • Attenuation compensation Q • 1D calibrated anisotropic velocity model

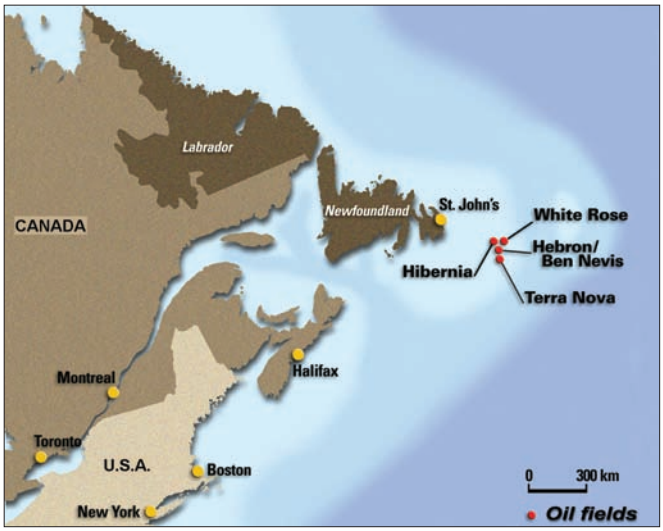

Figure 1. *Location of the White Rose Field.*

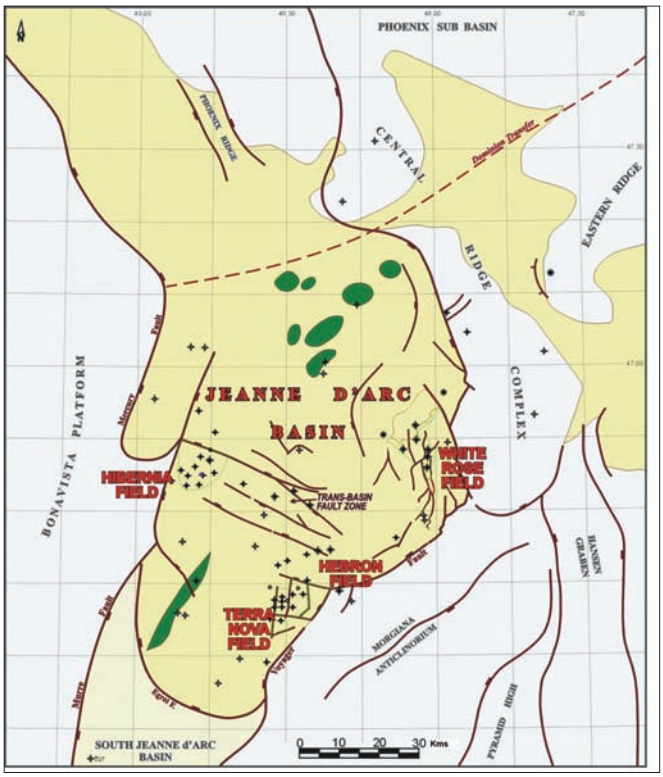

Figure 2. *The Jeanne d'Arc Basin showing location of the White Rose Field. Nomenclature from Enachescu (1987).*

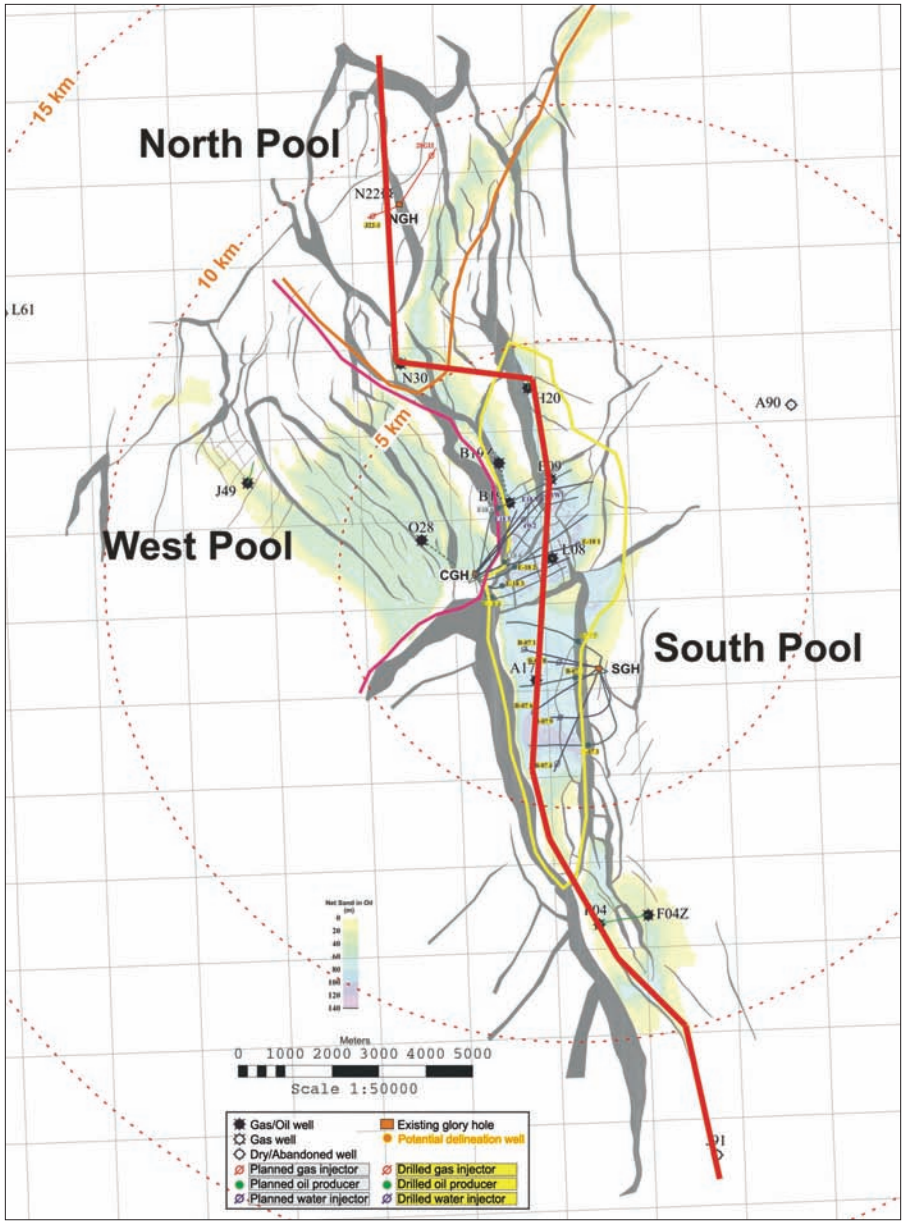

Figure 3. *Map of White Rose reservoir: Red line indicates cross-section in Figure 4.*

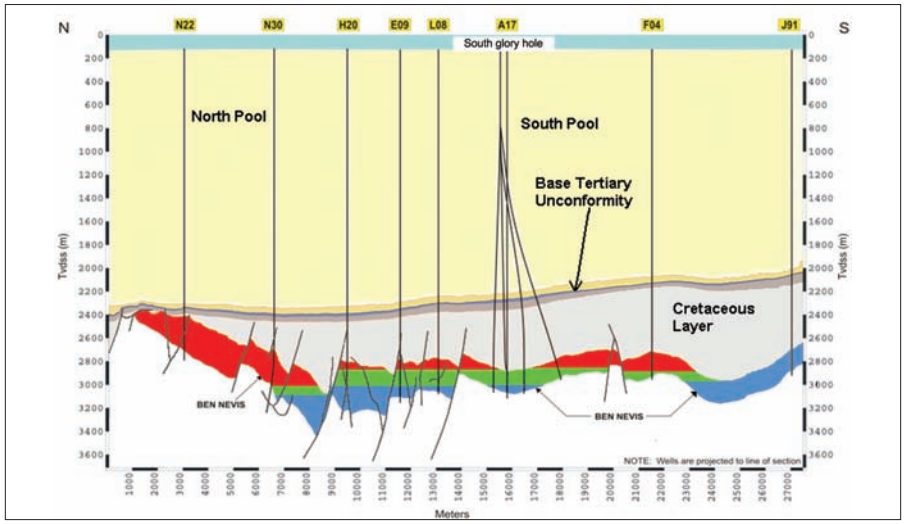

Figure 4. *Geologic cross-section showing faulting through the White Rose reservoir and gas (red), oil (green), and water (blue) zones.*

the red line shows the location of the cross-section in Figure 4.

Structurally, the White Rose area is complexly faulted, situated above a deep-seated salt ridge, and on the hanging wall of the Voyager fault. Faulting occurs throughout the reservoir at various scales, causing different degrees of compartmentalization (Figure 4). The producing reservoir is the Ben Nevis sandstone of mainly Aptian age, overlain by shales and mudstones. The sandstones are gas- and oil-bearing with thicknesses in excess of 200 m in some places.

The geology can be described in terms of two macrolayers, bounded by seismically resolvable unconformities and, correspondingly, internally consistent velocity responses. The first macrolayer, the Tertiary layer (which can essentially be considered the overburden), exhibits a layer cake sedimentary geology consisting of mostly mudstones and shales of the Banquereau Formation. These Tertiary sediments were deposited after the third and last phase of tectonic rifting during a period of extensive thermal subsidence (Enachescu, 1987; Sinclair, 1993).

The second macrolayer, the Cretaceous layer, is defined by the Base Tertiary unconformity and the mid-Aptian unconformity. Within this layer lies the Ben Nevis reservoir. The layer consists mainly of thin Dawson Canyon shales and limestones with thick Nautilus Formation shales overlying the reservoir. The layer is structurally complex, with evidence of extensional faulting during deposition of the Nautilus shales and Ben Nevis reservoir sandstone (Sinclair 1993).

Water depth in the region is approximately 100 m. In some areas, the seabed consists of large boulders and cobbles deposited by previous glaciation and a hard pan surface caused by early diagenesis.

Geophysical setting. The water bottom in the area is very hard, with a reflection coefficient of ~0.7 computed from VSP data (Figures 5 and 6). This very high reflection coefficient generates water-column reverberations that interfere with primary seismic reflections.

The Tertiary-Cretaceous boundary, just above the reservoir, generates a high-amplitude reflection event. It is an erosional unconformity with a strong acoustic impedance contrast. As a result, a significant amount of energy is reflected and subsequently trapped in the water column, pro-

Table 2. *Specific objectives with corresponding well contributions.*

Objective	Borehole contribution
Improve clarity of horizons and faults	Provide reliable velocity values throughout the processing route
Improve signal-to-noise ratio	Predictability and correlation with corridor stacks to confirm continual improvement throughout the processing sequence
Improve multiple removal	Calibrate 1D multiple modeling and well calibration
Account for anisotropy throughout processing	Determine η and apply in processing flow
Enhance resolution	Determine and apply Q
Maintain phase and amplitude consistency	Calibrate data to VSPs and sonic logs
Maintain AVO consistency	VSP and sonic log data to ensure accuracy when deriving rigorous offset and depth dependent gain functions

ducing strong cascading peg-leg multiples.

The Tertiary sediments are essentially a 2000-m stack of horizontally layered shales, which are expected to exhibit anisotropy. Inspection of the gather in Figure 13 shows the inability of an isotropic velocity function to adequately correct the long offsets, and the characteristic "hockey-stick" shape implies the presence of anisotropy.

The top of the reservoir has a very low-impedance contrast with the overlying shales, resulting in a very weak reflection. Seabed peg-leg multiples cascading from the Base Tertiary unconformity interfere with the reservoir reflection, making seismic picking and mapping challenging.

Extensional faulting at the reservoir level can locally propagate through the Base Tertiary unconformity. As a consequence, gas clouds are formed by updip leakage along such faults. The obscuring and distorting effects of gas clouds on the image are observed on some seismic data.

Underlying the Ben Nevis reservoir is the mid-Aptian unconformity, which is an angular unconformity throughout the White Rose area. The lithologic change at the unconformity gives rise to a strong acoustic impedance contrast and consequently a strong, though variable and discontinuous, mappable reflection.

Several reprocessing attempts were made in the past with limited success. Major objectives for this reprocessing initiative are shown in the left column of Table 2. For each objective, potential VSP and well contributions were formulated as summarized in the right column of Table 2.

Velocity model and anisotropy. As described earlier, in the White Rose area there is a thick (approximately 2000 m) depositional sequence, essentially a shale overburden, demarcated by the Base Tertiary unconformity, with reservoir targets 200–800 m below it. Shales, in particular, typically exhibit intrinsic transverse isotropy (TI), where seismic velocity is the same in all transverse directions parallel to bedding and slower in all other directions. Furthermore, if this shale sequence were to exhibit rotational invariance or transverse isotropy with a vertical symmetry axis, VTI, the azimuthal orientation of the measurements should be unaffected. Traveltimes measured for a source at fixed offset and receiver at fixed depth should be azimuthally invariant—i.e., they would be the same regardless of the orientation of the vertical plane containing the source and receiver.

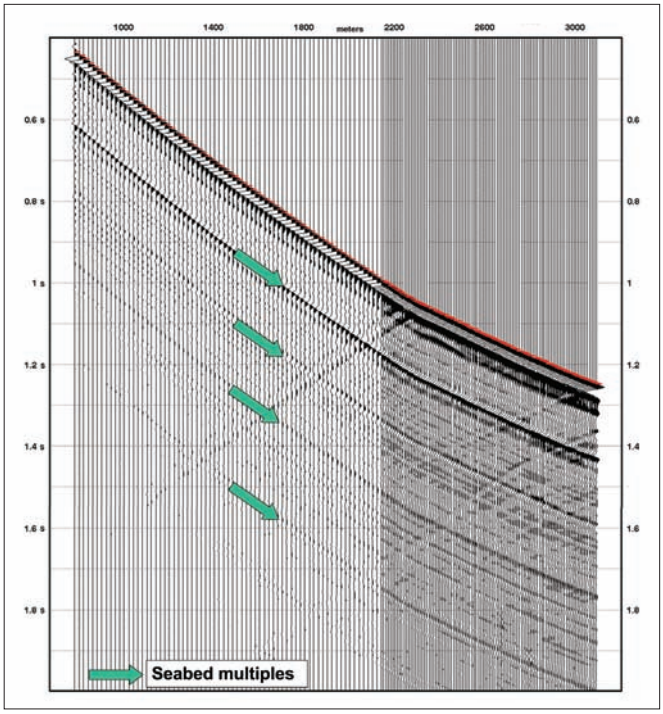

Figure 5. *VSP downgoing wavefield, aligned parallel to direct arrivals showing first-, second-, third-, and fourth-order seabed multiples.*

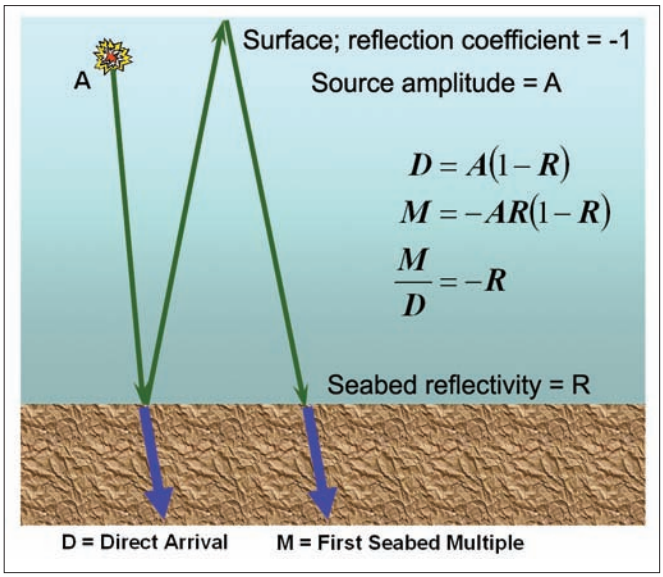

Figure 6. *Calculation of seabed reflectivity from ratio of multiple-to-primary amplitudes.*

It is often assumed in seismic data processing that the Earth is isotropic to the propagation of seismic waves, i.e., the velocity of propagation is independent of direction. Higher-order moveout terms are thus ignored. If anisotropy is large enough, the moveout becomes significantly nonhyperbolic, resulting in seismic sections having mispositioning errors and distorted structural images. In order to obtain seismic sections that are truer and more reliable representations of the Earth, anisotropy must be taken into account.

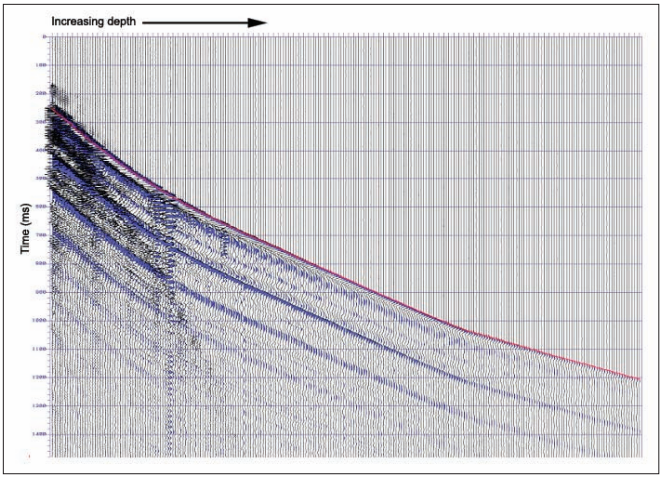

Figure 7. Zero-offset VSP with first-break times picked.

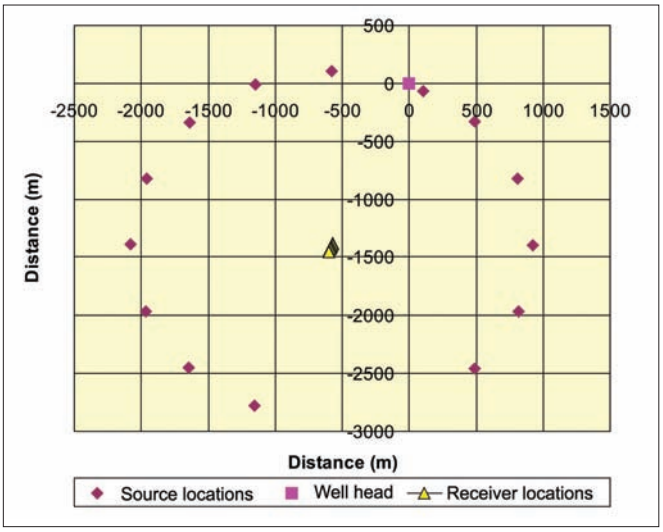

Figure 8. Walkaround VSP acquisition geometry, plan view.

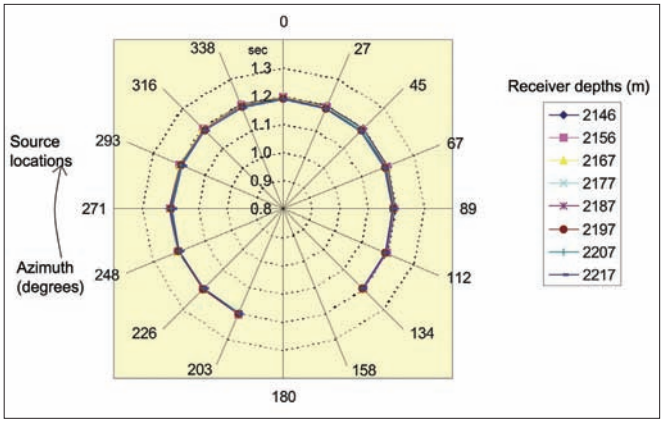

Figure 9. Geometry corrected azimuthal traveltime variations, normalized by receiver and source locations.

For production projects, it is important to precisely and accurately position the seismic images within or near a reservoir. A thorough knowledge of the elastic properties including anisotropy is required. Properly taking into account the effects of anisotropy results in sharper images that are positioned correctly. The accuracy of the images and the derivation and optimal determination of other critical processing parameters, such as vertical velocity gradients that impact migration of reflection data, is verified by the quality of the ensuing well ties. Understanding the nature of the velocity anisotropy improves depth estimations to seismic reflectors.

The best method available for in-situ determination of anisotropy parameters is the VSP. Azimuthal anisotropy can be determined by a walkaround VSP (WAVSP), and VTI by a walkaway VSP (WVSP). The walkaround VSP was acquired to assess the extent (or lack) of azimuthal anisotropy. The consistency of traveltimes with varying source direction confirmed that the azimuthal anisotropy was negligible, thereby allowing the possibility of using a walkaway VSP in an arbitrary direction for the determination of VTI elastic parameters, δ and ε (Thomsen, 1986).

VSP data acquisition for anisotropy determination. Well trajectories with VSPs in the field vary in geometry from vertical to ~60° deviation. Borehole seismic data were recorded in several. All data acquisition used 3-C sensors with multilevel array tools, progressing from three-level open-hole systems earlier on to the current 5- and 8-level arrays. A multiple-element tuned air-gun array at 6 m depth was the source.

In the well selected for anisotropy determination, three different types of VSPs were acquired: a normal-incidence (or walkabove) VSP, a walkaround VSP, and a walkaway VSP. The well was deviated, with the maximum deviation being 52.3°.

Normal-incidence VSP. The normal-incidence VSP was acquired at 15 m intervals from the bottom of the well to the surface. Shot locations were dynamically positioned above the center receiver of a 5-level array for each shot. On average, seven shots were recorded for each depth level. Geophone traces within each level were subsequently aligned and stacked to produce a single trace for each depth level. Figure 7 shows the *z*-component stack. Since the source is always nearly vertically above the receivers, ray paths are normally incident. Most particle motion is in the vertical plane so only the vertically polarized component data were utilized.

Walkaround VSP (WAVSP). Data for the walkaround VSP were acquired in a circular pattern, with a nearly constant radius of 1.5 km (Figure 8). The center of the circle was positioned above the middle of the central geophone of an eight-geophone array string, at a fixed depth just above the Base Tertiary unconformity. A single shot was acquired at each location. Sixteen shot locations were planned, but two could not be acquired due to operational considerations. Figure 9 shows the final compensated traveltimes for each azimuth and each receiver.

The measured traveltimes were corrected for geometry by accounting for the differences in travel-path length due to: varying source offset, varying receiver depth, and varying receiver offset along the deviated borehole.

The results of the walkaround VSP are indicative of an azimuthally invariant medium between the surface and the receiver.

Walkaway VSP (WVSP). Figure 10 is a plan view of the walkaway survey geometry. Shot lines were centered over the receiver array depth range, and three closely overlaying shot lines were acquired, aligned close to the structural strike. Each line consisted of 200 shot locations with a shotpoint interval of 25 m, with maximum source-receiver off-

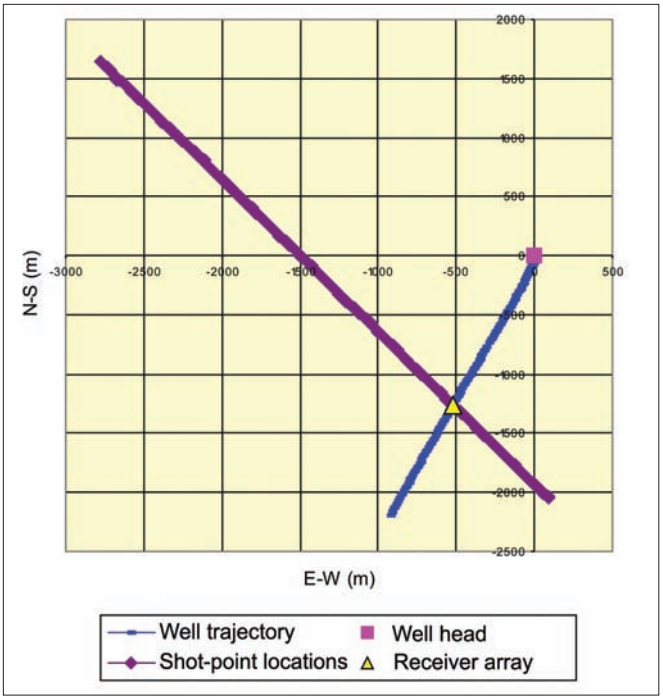

Figure 10. Plan view of walkaway VSP survey geometry. The angle between the well trajectory and shot lines is 61°. The wellbore inclination is 46° at the center of the receiver array.

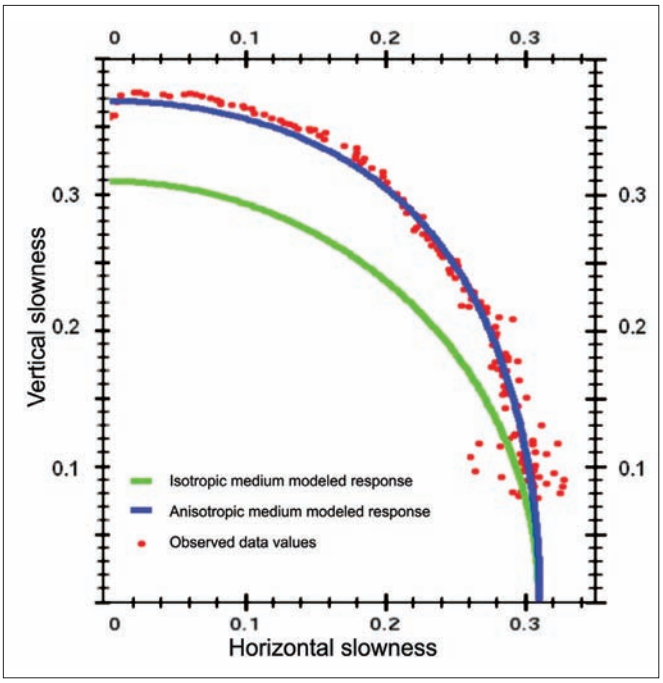

Figure 11. Horizontal and vertical phase slowness.

sets from the center of the receiver array of 4000 m and 1000 m, as shown. Receivers consisted of 3-C geophones configured in a 5-level array, with a spacing of 15 m between the geophones.

The combined receiver array consisted of 15 levels and covered a vertical depth range of 1980 –2123 m with an interval of 143 m. The shot lines were oriented 61° from the well trajectory. The surveyed well was deviated 46° from vertical at the array center and aligned with the structural dip. The center of the array was positioned just above the base Tertiary boundary, at a depth of 2051 m.

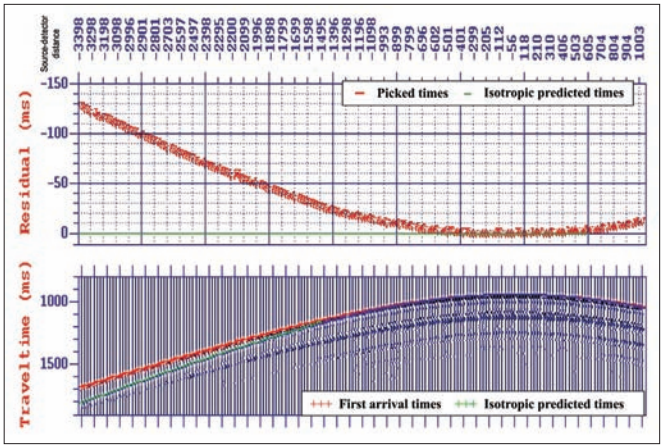

Figure 12. Traveltime residuals between real walkaway VSP data and times predicted by an isotropic (green) and anisotropic (red) overburden.

Data processing and anisotropic effect. Walkaway data can be used in several ways to derive anisotropic parameters (Zhou and Kaderali, 2006). Local elastic parameters at the receiver array may be determined by the horizontal and vertical phase-slowness method (Miller and Spencer, 1994), or by the slowness-polarization method (Horne and Leaney, 2000). Alternatively, estimates of the anisotropy profile above the receiver array can be made either by treating it as an effective medium or by a tomographic traveltime inversion approach constrained by the known vertical velocities at the wellbore.

In the horizontal-to-vertical phase slowness method, the main assumption is that the overburden is laterally homogeneous. If that condition is honored, the horizontal slowness at the receiver depth can be calculated from the time-difference and offset-difference between successive source points on the surface. The vertical slowness can be found from the traveltime differences across the receiver array. Figure 11 shows this kind of crossplot, together with the horizontal versus vertical phase slowness that would be expected for an isotropic medium (green) and the surface that was modeled from the inversion result (blue) for an anisotropic medium.

It is important to note that this is a measurement of the local elastic moduli at the depth of the receiver array. In general, anisotropy increases with depth of burial, so that shallower depths in the overburden are expected to exhibit less anisotropy.

Figure 12 shows the results of deriving anisotropy from the walkaway VSP by traveltime inversion. The initial velocity model was derived from the vertical velocities from logs and normal incidence VSP traveltimes. The residuals between the measured traveltimes and those predicted from the model using isotropic layers are shown by the red curve. At the farthest offsets of the walkaway VSP (~4 kms), the isotropic velocity model predicts traveltimes delayed by up to 160 ms compared with the observed data.

The red curve shows the residuals when a constant ε and δ are used for the entire overburden. Alkhalifah and Tsvankin's parameter, η, (1995), a measure of the deviation of long-offset P-wave moveout from what it would have been for an isotropic medium, can be obtained from δ and ε using the relationship:

$$\eta = (\varepsilon - \delta) / (1 + 2\delta)$$

Using this formula, a value for η of 0.137 was derived as a representative vertical average for the Tertiary section

Table 3. *Demultiple strategy comparisons.*

Strategy	Application assessment in White Rose
Velocity/moveout discrimination (e.g., parabolic Radon transform)	Removes seabed multiples, but less effective on peg-legs with moveouts close to primaries
Structural discrimination	Discrimination of conflicting primary/multiple dips, below base tertiary
Predictability using models [e.g., surface-related multiple elimination (SRME)]	Removes interbed multiples. Shallow water depth and hard water bottom affects the outcome
Predictability using periodicity (e.g., deconvolution)	Removes water-bottom multiples. Inconsistent in structurally complex zones (e.g., below base tertiary)

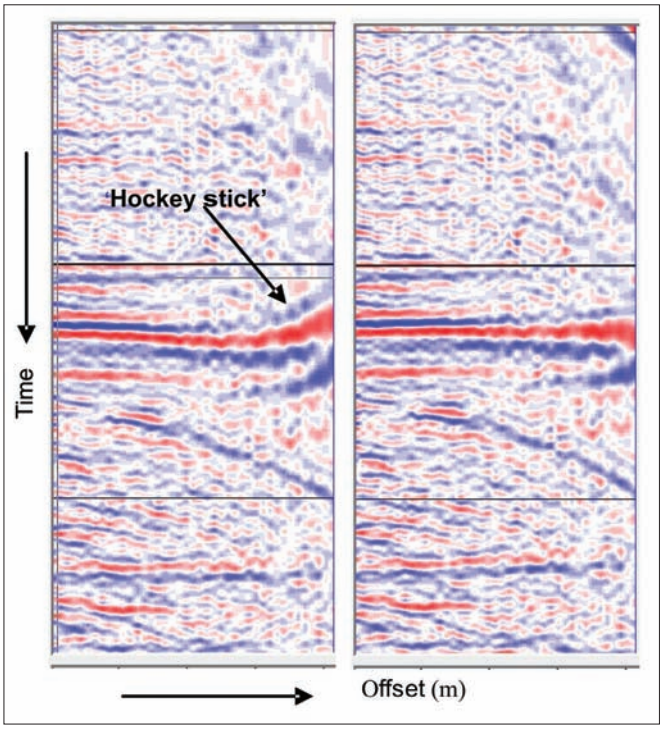

Figure 13. *Gathers showing the effectiveness of the anisotropy correction (left no correction, right with correction).*

over the whole survey. This value was imposed on all velocity analyses carried out on the surface seismic volume.

An immediate benefit of incorporating anisotropy in the velocity function can be seen in Figure 13. A CDP gather is shown on the left with moveout correction using an isotropic velocity function. The best velocity determination still leaves residual moveout at the longer offsets, the hockey stick effect, clearly visible at the strong Base Tertiary reflector. The same gather is shown on the right after the VSP-derived anisotropic term is included in the moveout correction. The Base Tertiary reflector is now accurately corrected. This has two major benefits: improving the stack response of the gather, and allowing the use of longer-offset traces for AVO.

The multiple problem. For this data set, multiple attenuation or removal is even more critical than in many other

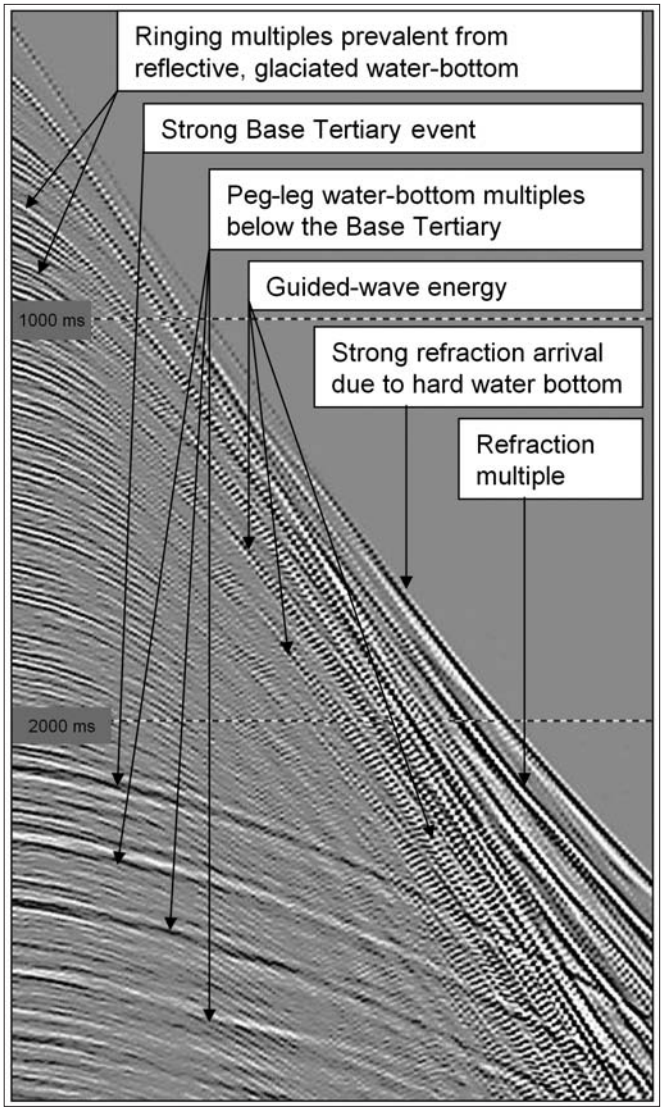

Figure 14. *A typical shot from the 1997 survey. The peg-leg multiples beneath the highly reflective Base Tertiary event obscure the primary (see Figure 15).*

marine areas because of the hard water bottom. A number of different strategies were assessed, some of which are listed in Table 3.

Seabed multiples are widespread in the shallow zone, above the Base Tertiary. Water-bottom peg-leg multiples overlie the zone immediately below the strongly reflective Base Tertiary (Figures 14 and 15). Most strategies listed in Table 3 were attempted previously with varying degrees of success (Figure 16).

For this survey, a combination of strategies produced the best results. The determination of the parameters for each strategy, and the combination and order in which they were applied, were fully investigated and an effective approach developed.

All possible peg-leg multiples generated from modeled interfaces can be predicted from a calibrated 1D model. These can be displayed, indexed according to their moveout velocities, and overlain with the primary moveout velocities for comparison. Examples for a well from the area are shown in Figure 17. The following inferences may be made:

- Strong first-order and second-order water-bottom multiples indicate that model-based predictability strategies

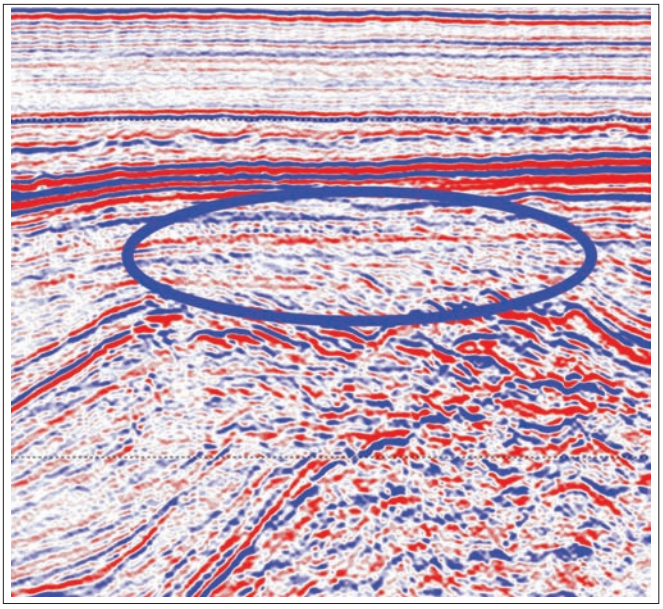

Figure 15. *A brute stack from the area. Note the strong horizontal peg-legs obscuring the main zone of interest (highlighted).*

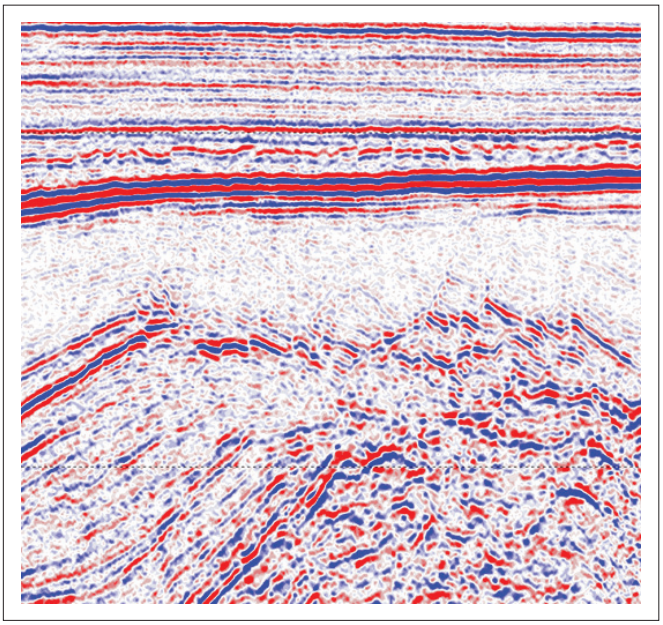

Figure 16. *A previous reprocessing attempt, using mainly structural discrimination strategies. The peg leg multiples have been effectively removed, but with coincident attenuation of primaries.*

should produce good results in the shallower data.

- Although there are no peg-legs faster than the primary data, velocity discrimination is negligible. Velocity-based demultiple methods will be unable to differentiate between primary and multiple signal.
- Interbed multiple contamination is evident in the target zone, indicating that model-based methods should also include other multiple generating horizons.

Well information was also used to assess the effectiveness of the demultiple pass based on velocity discrimination (Figures 18 and 20). Modeling of the multiples showed that residual multiples remained even when a normal-moveout correction of 96% of the primary velocities were used for multiple rejection.

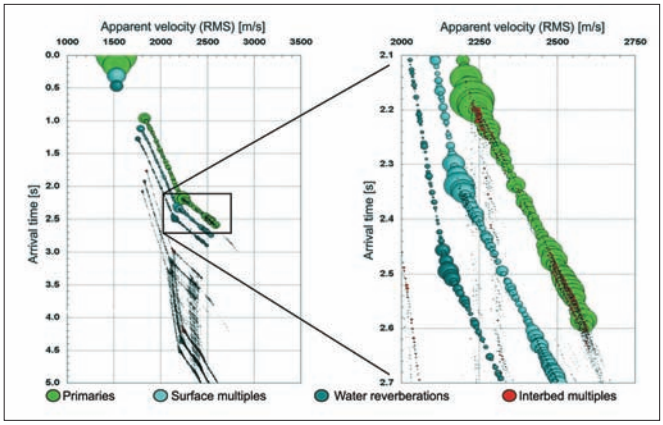

Figure 17. *Calibrated 1D model at well N-30 showing primary data and all possible multiples generated from the modeled interfaces. The radii of the circles correspond to the predicted amplitude of the events. The enlargement on the right focuses on the main zone of interest. There are strong surface multiples from 2.3 s onward and reverberations from 2.45 s, and frequent interbed multiples from 2.2 s downward.*

A synthetic shot gather was derived by finite-difference elastic modeling of a detailed velocity (P and S) and density profile at well L-08. This model also included the very strong seabed reflectivity. The synthetic was examined after each stage of the demultiple application to assess the predicted effects of different demultiple strategies (Figure 19). This approach can be used at any stage in the processing sequence to provide guidance for the most effective strategies to pursue, whether they be for demultiple or other steps.

Q determination. Correct amplitude and high-frequency recovery are crucial in the interpretability of the seismic data because of the depth of the target zone and its location below the highly reflective Base Tertiary unconformity. Compensating for attenuation (Q) factors is thus a vital component of data processing in this area. Q values were determined at several well locations using various methods.

Q may be determined using the spectral ratio analysis method (Leaney, 1999). Amplitude spectra are compared for wavelets that have propagated different distances through the medium to be measured. In the VSP case, the downgoing wavefields recorded at different depths in the Earth (i.e., different geophone depths in the well) are the appropriate input data for such an analysis. Figure 21 shows the spectra for a wavefield recorded at a shallow (red) and a deep (green) depth in the earth.

The logarithm of the ratios of the spectra is taken frequency by frequency and plotted as the blue curve in Figure 21. The slope of the best fit line (magenta) over the expected frequency range of the signal (in this case 5–90 Hz) gives an estimated Q value of 100.

This approach can be extended to every combination of pairs of depths. The Q value for each depth pair is plotted with respect to the midpoint depth of the pair (Figure 22). The degree of confidence in the spectral slope is color-coded, with red representing the highest confidence. Although there is a large variation in derived Q values, those in red are distributed fairly consistently in the range from 100 to 110.

The spectral ratio analysis method measures the preferential attenuation of high frequencies in the data as a function of propagation distance. Another method, waveform coherency analysis, is concerned with the effect of Q on the shape of a pulse as it passes through a dispersive medium. The downgoing VSP wavefield is corrected by inverse Q fil-

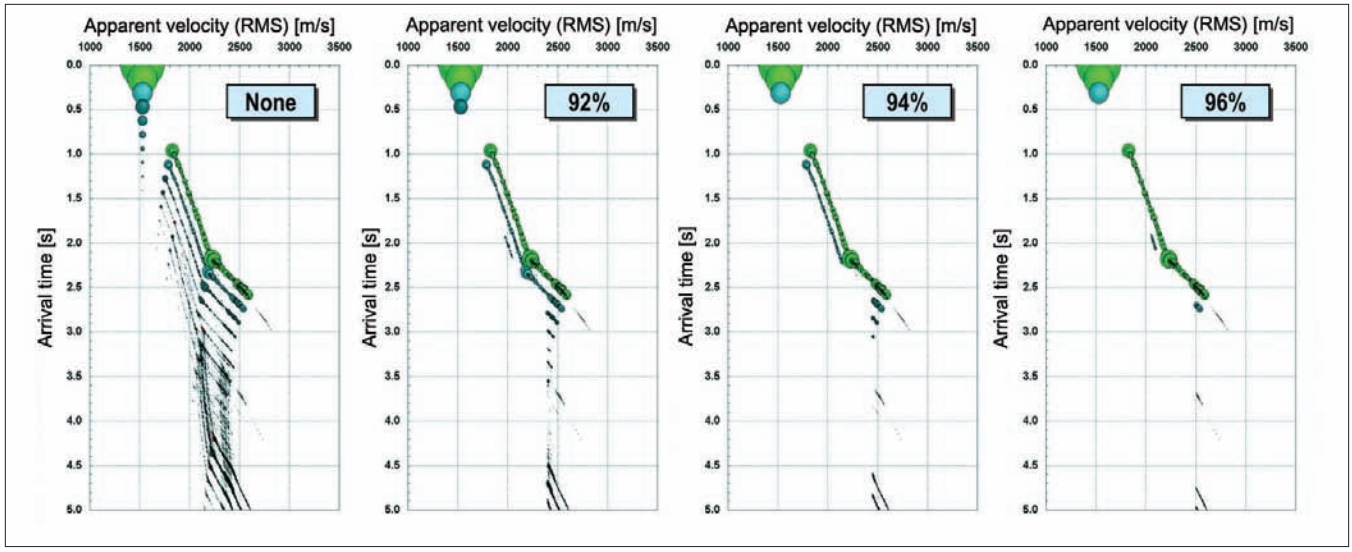

Figure 18. Different velocity discrimination demultiple applied to the calibrated 1D model from N-30. Residual demultiple energy remains even when the NMO discrimination is as high as 96% of the velocity function of the primary reflectors. See also Figure 20.

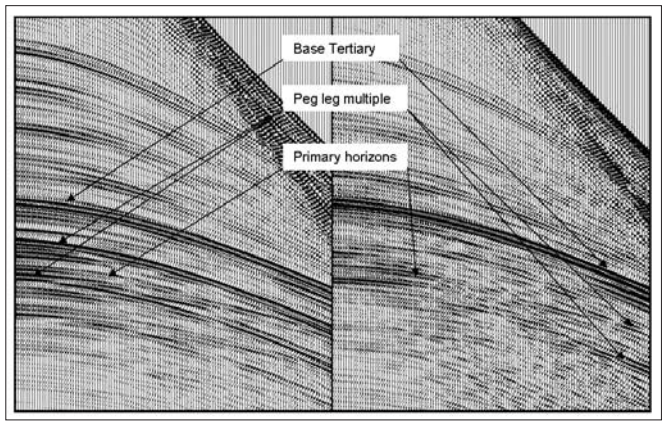

Figure 19. A synthetic gather derived from well data, shown without demultiple (left) and after a τ-p demultiple deconvolution (right).

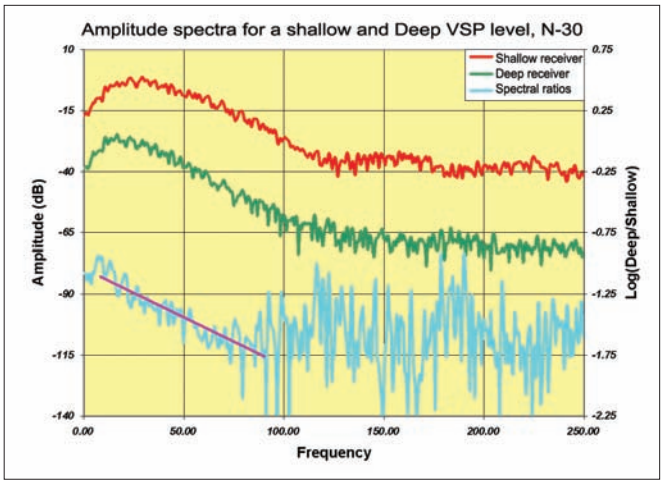

Figure 21. Amplitude spectra from different levels, shallow (red) and deeper (green). Spectral ratio (blue) of the two amplitude spectra is obtained by taking the logarithm of (deep curve/shallow curve). The best-fit line (magenta) over the curve between 5 and 90 Hz corresponds to a value for Q of approximately 100.

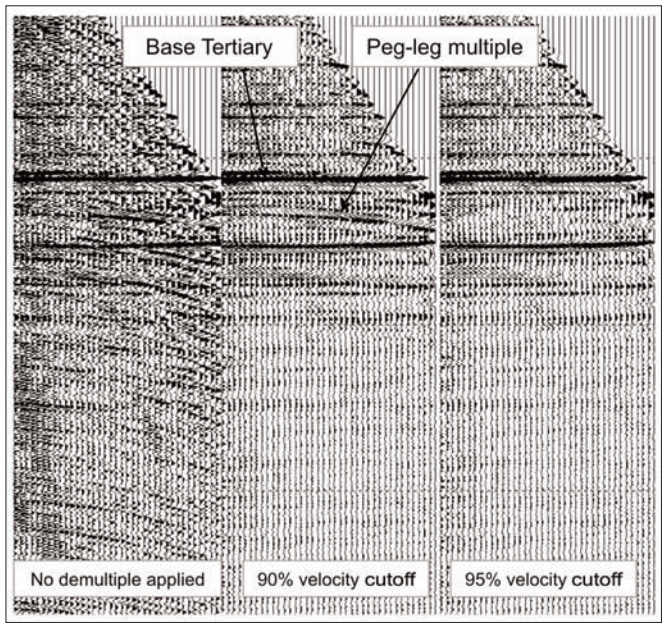

Figure 20. A gather before velocity-based demultiple and with 90% and 95% velocity cutoffs applied.

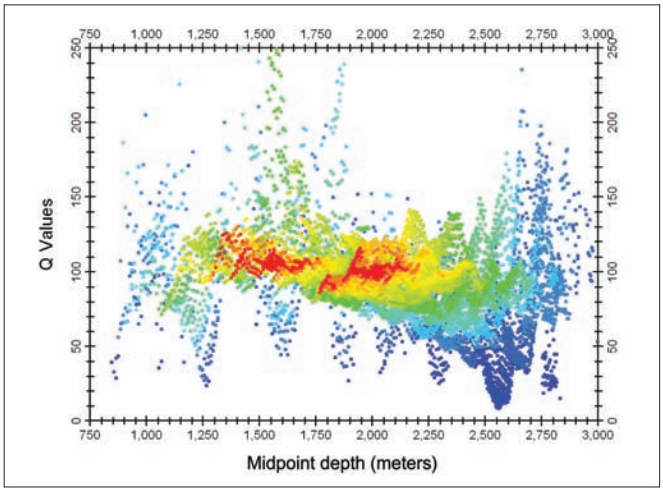

Figure 22. A multispectral ratio analysis of well N-30, with Q values plotted vertically against receiver pair midpoint depth. The colors show degree of confidence in the result with best Q values of approximately 105.

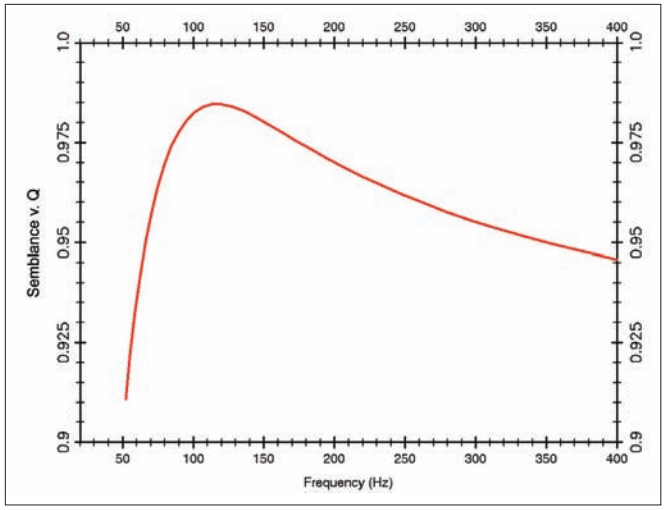

Figure 23. *Waveform coherency analysis of well N-30 showing a semblance maximum at Q = 110.*

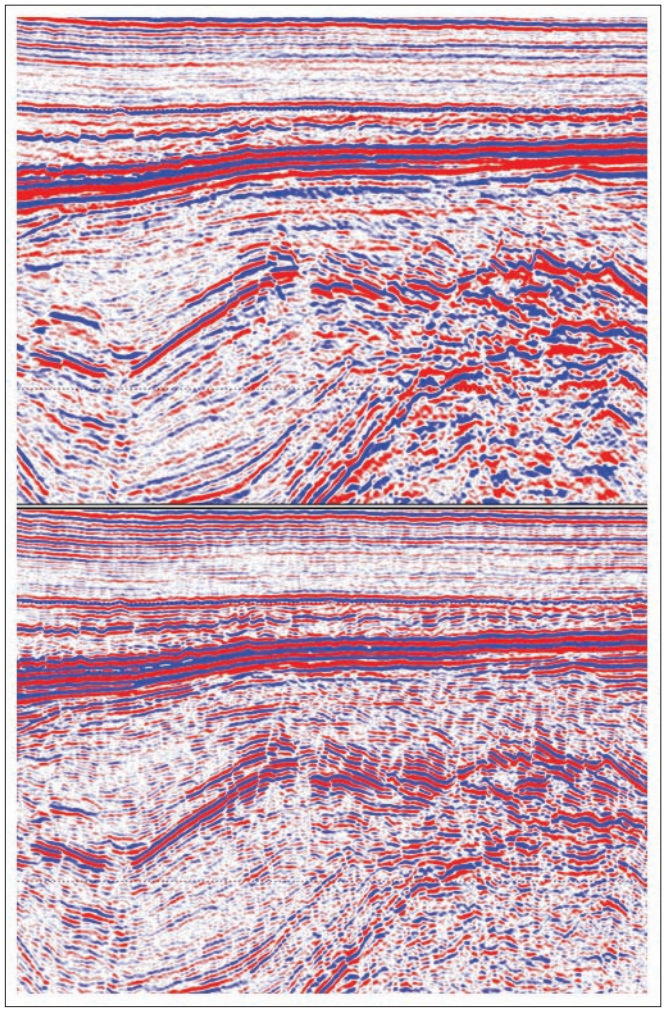

Figure 24. *An inline before (above) and after (below) inverse Q compensation. The latter shows improvement in frequency, resolution, and structural definition.*

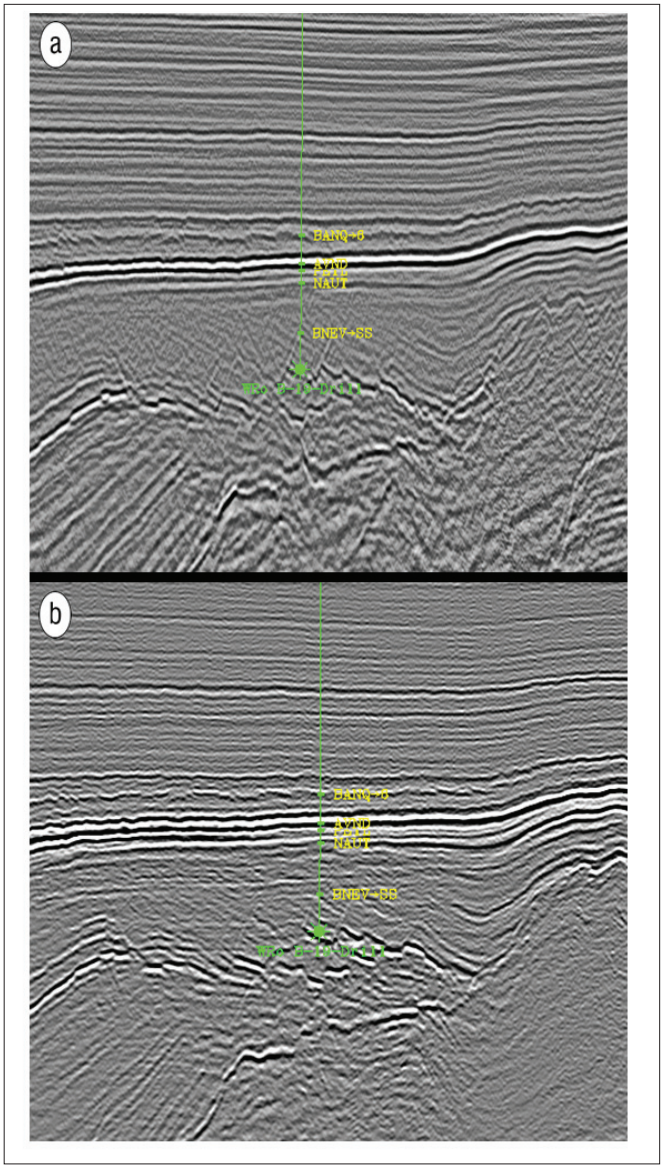

Figure 25. *Previous processing (a), early reprocessing result (b), showing the value of anisotropic migration. Resolution, imaging, and fault definition are improved.*

ters for a series of different values of Q. For each corrected version of the wavefield, the semblance is measured and used as an indicator of wavelet shape consistency. For the correct inverse Q filter, the traces will all have the same shape and the semblance across all depths will be a maximum. Figure 23 shows semblance versus Q, with the maximum value once more in the same range of approximately 110.

Utilization of borehole data provides values of Q in a more rigorous manner than the common method of applying a range of Q values to the surface seismic data and making a subjective selection. Having a reliable borehole-derived value allows flexibility in deciding at what stage in the processing to apply the attenuation factor, and whether to apply the phase and amplitude components separately or together. The application can also be quantitatively assessed by the inspection of before and after well ties. Figure 24 shows the effects of applying the amplitude and phase components of borehole-derived Q compensation to a White Rose line and the consequent improvement in frequency, resolution and structural definition.

Verification of data improvement. Improvements in the data volume need to be assessed continually to arrive at the optimal data processing parameters and flow. The best approach is to consider the agreement of the seismic response with the observable expression of the geology in the well logs and the

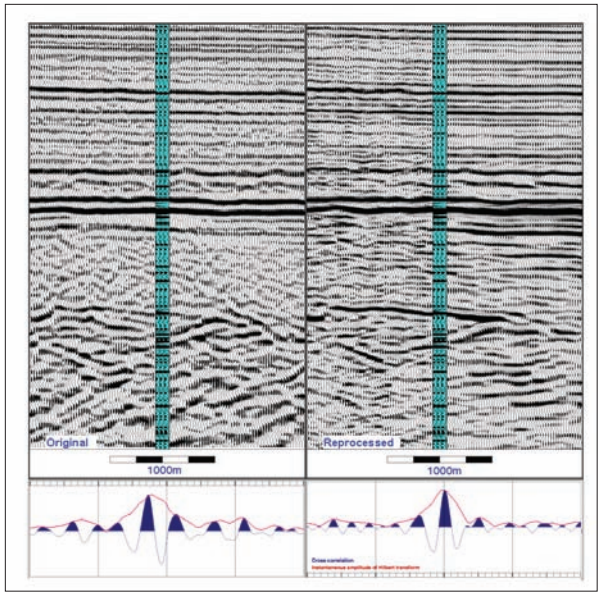

Figure 26. *Previous processing (left) and reprocessing (right) showing VSP corridor stack tie. Cross-correlations/Hilbert transform phase analysis. Zero-phase and character matching as well as event continuity are all improved.*

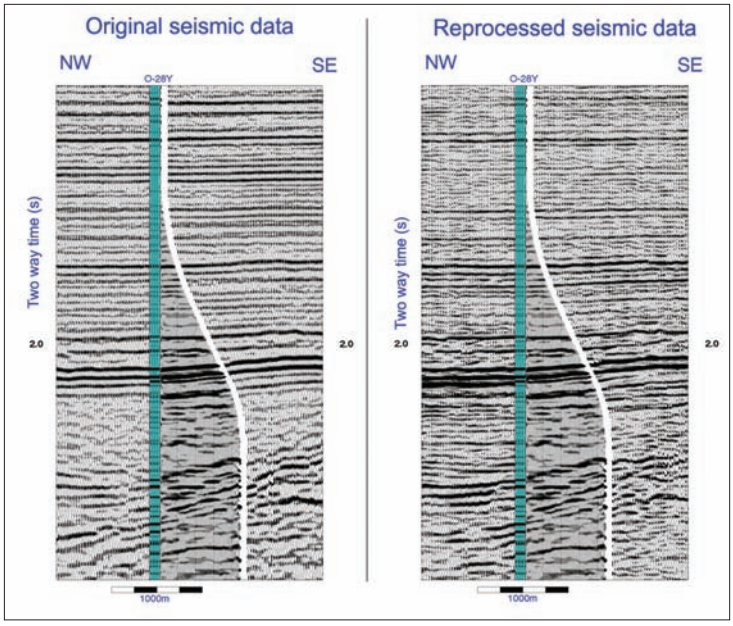

Figure 28. *Zero-offset VSP corridor stack and a walkabove image inserted in the seismic data. Information from this well was not used in reprocessing the seismic data.*

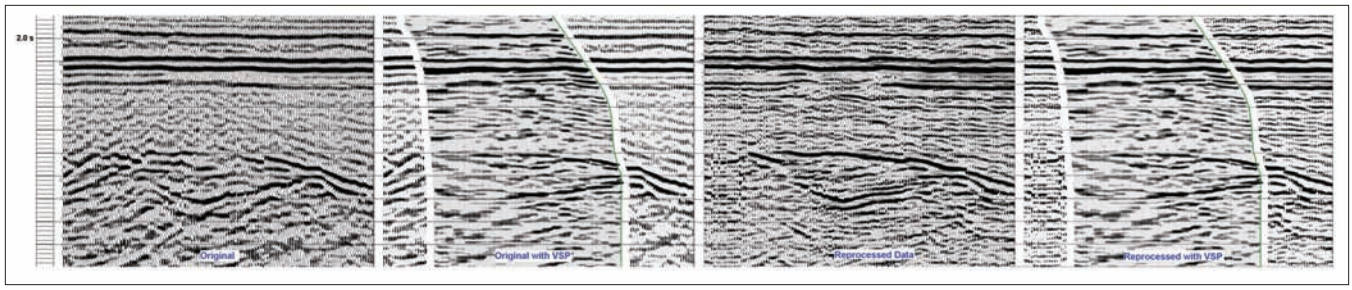

Figure 27. *Walkabove VSP image inserted into seismic data. Notice improved match, especially along well trajectory (green) with reprocessed seismic data.*

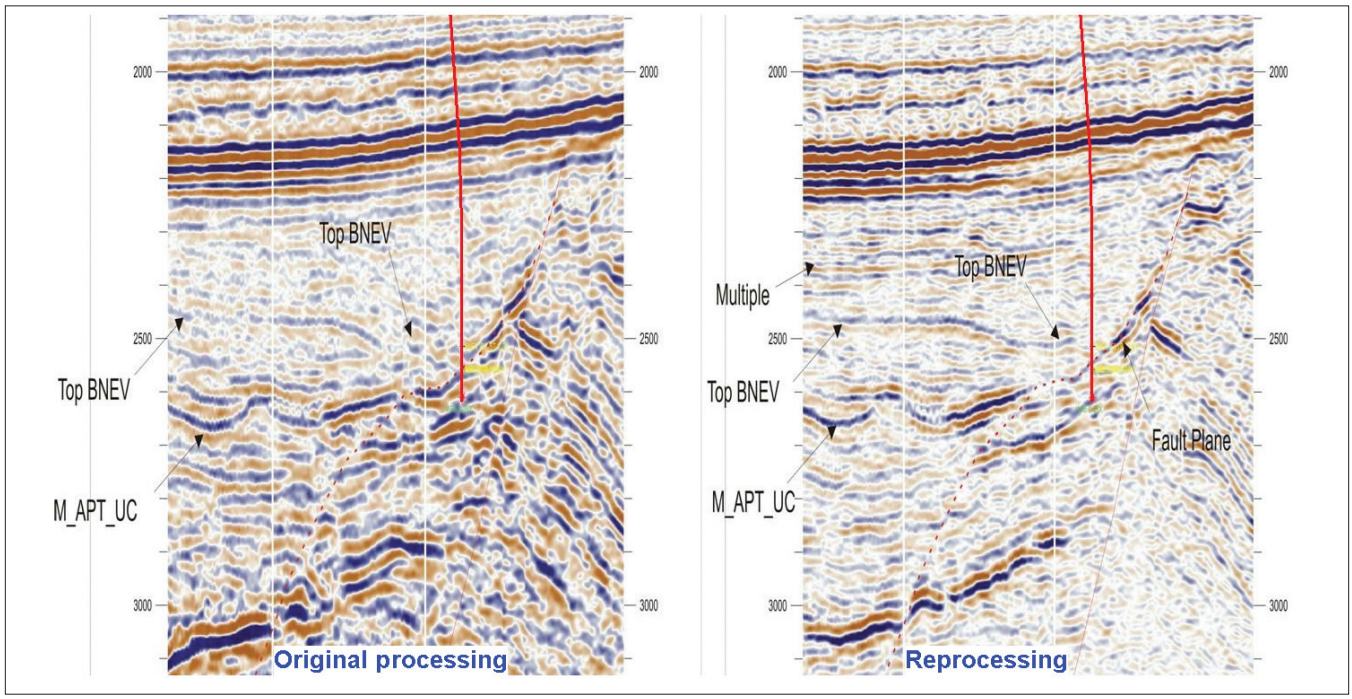

Figure 29. *Old (left) and reprocessed (right) sections. Top of reservoir (Top BNEV) and the base of the reservoir (M_APT_UC) now truncate against fault.*

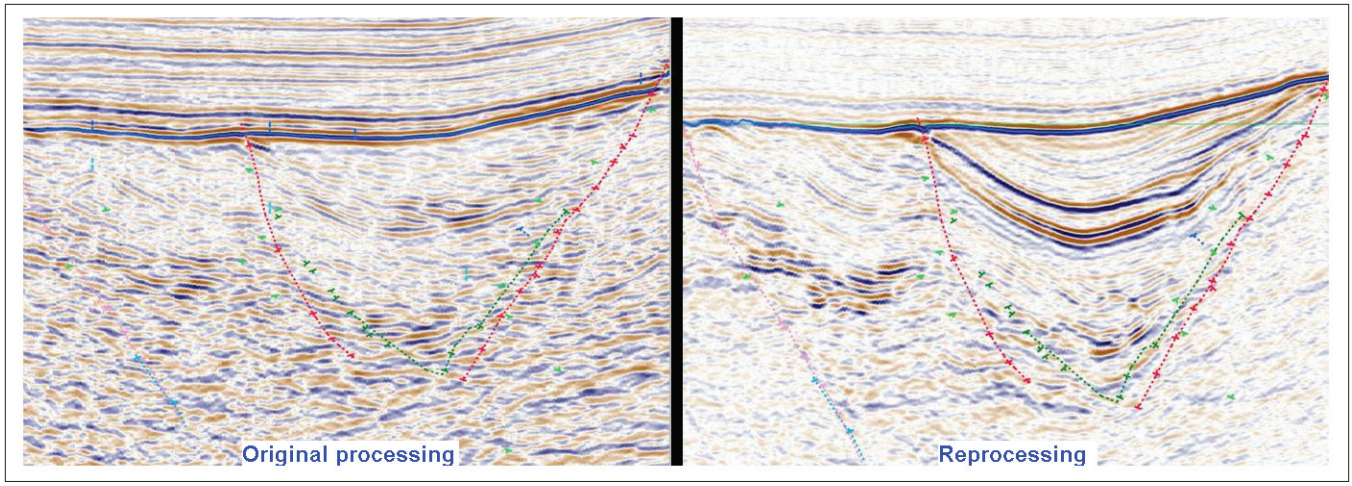

Figure 30. *A clear example of improvement in a prospective area obtained using borehole constrained reprocessing.*

borehole seismic. The following examples demonstrate that the reprocessed data match the geology at the control points provided by boreholes within the survey area.

As shown in Figures 25a and b, a provisional data volume utilizing the borehole derived anisotropy parameters showed a significant improvement in data resolution, even though multiple attenuation, inverse Q compensation, and other parameters had not yet been finalized. By comparing to a recently drilled well that was not used to constrain the data reprocessing, it was clear that the reprocessed data were more reliable than any previous data.

Despite residual multiple energy in the zone of interest in this early version of the reprocessing, events related to the reservoir zone can be better discerned and are in agreement with the well. Resolution, imaging, and fault definition have improved. The shallow zone above the Base Tertiary event, for which the "effective" anisotropy parameters were determined and applied, has increased lateral continuity.

Improvements in the reprocessed data are confirmed also by comparing line ties to VSP data. Three examples from different wells are shown. Figure 26 shows a VSP corridor stack tied to the original and reprocessed seismic data. Also shown are cross-correlations of the corridor stack with the corresponding seismic trace, plotted inside the invariant amplitude envelope obtained by taking a Hilbert transform. The cross-correlations show the reprocessed data to be a closer match to the VSP. The data are now closer to zero-phase and require minimal time correction. The tie with the corridor stack has improved considerably and primary events have better continuity.

Figure 27 shows the image from a walkabove VSP, acquired elsewhere in the survey, inserted into the seismic data. The VSP image, which has higher resolution due to the shorter ray-path geometry, is a closer match to the reprocessed data than the original data, especially along the trajectory of the well.

Figure 28 shows a zero-offset VSP corridor stack and a walkabove image inserted into the seismic data. This location was selected on the original data, and information from this well was not used in the reprocessing. It thus serves as an independent check of the reliability of the reprocessed data. The well was drilled vertically and subsequently sidetracked, making it possible to have both a zero-offset and a walkabove VSP. Like the earlier examples, there is a much better match with the reprocessed data in terms of well ties, resolution and continuity of events.

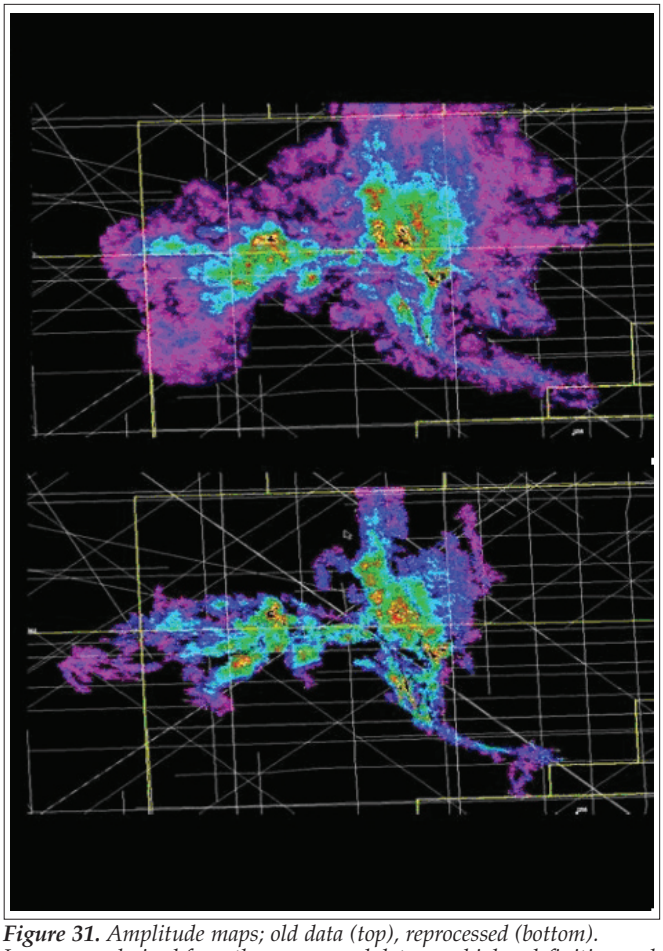

Figure 31. *Amplitude maps; old data (top), reprocessed (bottom). Lower map derived from the reprocessed data was higher definition and shows far less lateral smearing of amplitudes.*

The key to efficient exploitation of White Rose Field is in the placement of the wells. The main tool we have here is seismic. If the seismic is to be trusted away from well locations, it is imperative that the reprocessed seismic data agrees with the existing well information. This is not a new idea, but is often neglected.

As shown above, not only do the data now demonstrate superior well ties, they also provide improved structural resolution, fault definition, and event continuity. Additionally, the reprocessed data honor subsequently drilled wells that

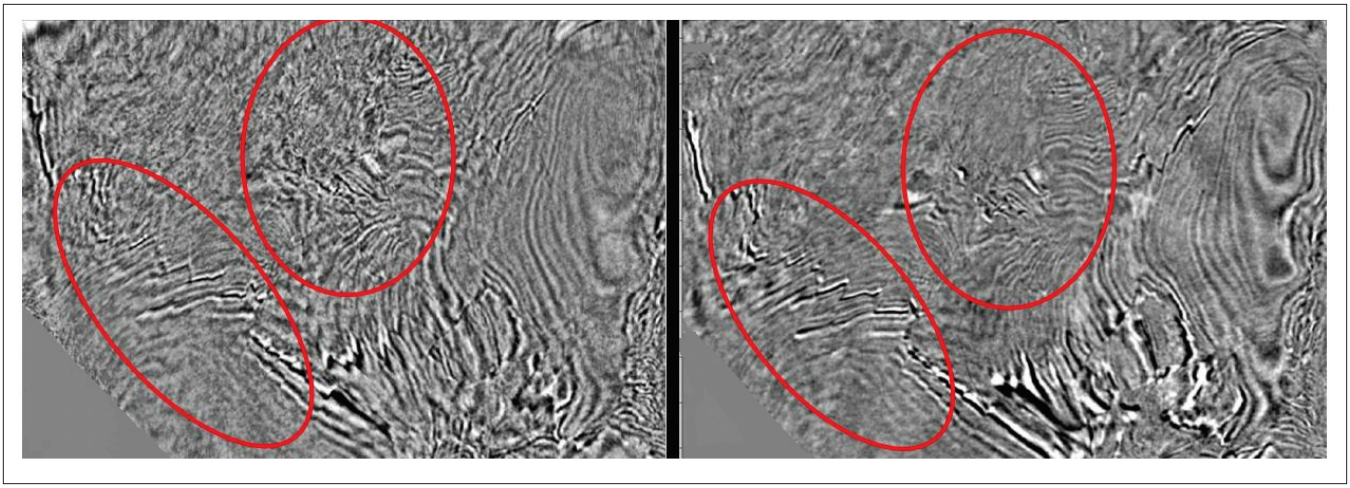

Figure 32. *Time slices showing improved lateral resolution and clarity. Original processing (left) and reprocessing (right).*

were not used in the reprocessing analyses, and so should enable a more confident and reliable interpretation.

Impact on interpretation. Interpreters familiar with this area have provided further confirmation of the improvements observed in the reprocessed data. Some examples, from different interpreters and different parts of the survey, are discussed below.

Figure 29 is an example of how the interpretation changed. On the original data, the top of the reservoir appears to dip and truncate, and the base appears to have a fairly consistent amplitude response and dips steeply. The reprocessed data lead to a different interpretation: the top and base truncate against a fault plane, as verified by a subsequently drilled well at the location shown on the section by a red line.

The next example (Figure 30) clearly shows improvement. Previously obscured prospective events are now evident. Better amplitude control during the processing has enabled a more confident stratigraphic and structural interpretation.

As shown in Figure 31, amplitude maps generated from the new data also show much better resolution than on the original data. The amplitude maps were derived by using an automatic picking algorithm through both data volumes. The lower map based on the reprocessed data has higher definition, shows far less lateral smearing of amplitudes and illustrates better defined potential targets for drilling and reserves calculations.

Another way of comparing data is by time slices (Figure 32). The reprocessed data show far better fault definition, and the red ellipses highlight areas with improved lateral resolution and clarity.

Conclusions. These examples demonstrate that it is essential to honor and incorporate well information in the processing of surface seismic data. If the seismic data are to be trusted away from the well locations, at the very least they must agree at the well locations.

Borehole seismic data provide the necessary bridge, directly and indirectly, between the geologic section and its seismic response. They allow direct measurement of anisotropy, velocity, dispersion, prediction and identification of multiples, and the testing of the effectiveness of various processes applied to the seismic.

Anisotropy, a key parameter, is most effectively measured in-situ by a walkaway VSP. Other processing parameters can then be optimized using VSP information. Significantly improved seismic images are obtained as a consequence, and the seismic data have been demonstrated to be more reliable. There has been a positive impact on development by enabling better placement of wells. This has had, and will continue to have, an impact on future development at the White Rose Field.

Suggested reading. "Velocity analysis for transversely isotropic media" by Alkhalifah and Tsvankin (GEOPHYSICS, 1995). "Tectonic and structural framework of the northeast Newfoundland continental margin" by Enachescu (in *Sedimentary basins and basin-forming mechanisms*, Canadian Society of Petroleum Geology Memoir 12, 1987). " Polarization and slowness component inversion for TI anisotropy" by Horne and Leaney (*Geophysical Prospecting*, 2000). " Walkaway Q inversion" by Leaney (SEG 1999 *Expanded Abstracts*). "An exact inversion for anisotropic moduli from phase slowness data" by Miller and Spencer (*JGR*, 1994). "Tectonism: The dominant factor in mid-Cretaceous deposition in the Jeanne d'Arc Basin, Grand Banks" by Sinclair (*Marine and Petroleum Geology*, 1993). "Weak elastic anisotropy" by Thomsen (GEOPHYSICS, 1986). "Anisotropy evaluation using an array walkaway VSP" by Zhou and Kaderali (OTC-18177-PP, 2006). TLE

Acknowledgments: From Husky Energy, Larry Mewhort for his support, encouragement, and technical reviews; Andrew Churchill, Judith McIntyre, Lyndon Miller for providing the interpretation examples; Iain Sinclair and Craig Lamb for reviewing the paper. From Schlumberger and WesternGeco, Richard Parker, Josef Heim, Nick Wood and his group for processing the data. We thank Wendy Mewhort for her help with the manuscript. The authors also thank Husky Energy for permission to publish this paper.

Corresponding author: Ayiaz.Kaderali@huskyenergy.ca

JUNE 2007 THE LEADING EDGE 000